LBNL-39269
UC-414
Preprint

ERNEST ORLANDO LAWRENCE
BERKELEY NATIONAL LABORATORY

β-Decay and Cosmic-Ray Half-Life of ^{54}Mn

T. Kibedi, M. Kerr, E.B. Norman,
G.D. Dracoulis, and A.P. Byrne
Nuclear Science Division

August 1996
Submitted to
Astrophysical Journal

LBNL-39269
UC-414

β-Decay and Cosmic-Ray Half-Life of ^{54}Mn

T. Kibedi,[1] M. Kerr,[1] E.B. Norman,[2] G.D. Dracoulis,[1] and A.P. Byrne[1]

[1]Department of Nuclear Physics
Research School of Physical Sciences and Engineering
The Australian National University
Canberra, ACT 0200, Australia

[2]Nuclear Science Division
Ernest Orlando Lawrence Berkeley National Laboratory
University of California
Berkeley, California 94720

August 1996

This work was supported by the Director, Office of Energy Research Division of Nuclear Physics, Office of High Energy and Nuclear Physics, of the U.S. Department of Energy under Contract No. DE-AC03-76SF00098.

β^--DECAY AND COSMIC-RAY HALF-LIFE OF ^{54}Mn

T. Kibédi[1], M. Kerr[1], E. B. Norman[2], G. D. Dracoulis[1] and A. P. Byrne[1]

Submitted to *Astrophysical Journal*

6 August, 1996

ABSTRACT

A superconducting solenoid electron spectrometer operated in the lens mode was adapted to search for the β^--decay of ^{54}Mn. The Compton-electron and other instrumental backgrounds were largely reduced by special shielding of the absorber system. An improved procedure was developed to select the events by momenta. An upper limit of $<2.7 \times 10^{-5}$ has been established for the intensity of the β^- branch. This would define the partial half-life of the ^{54}Mn β^--decay to be greater than 3.2×10^4 years. The implications of this result for the ^{54}Mn cosmic-ray chronometry problem are discussed.

[1] Department of Nuclear Physics, Research School of Physical Sciences and Engineering, The Australian National University, Canberra, ACT 0200, Australia
[2] Nuclear Science Division, Lawrence Berkeley National Laboratory, Berkeley, CA 94720, USA

1. INTRODUCTION

Cosmic-ray isotope measurements offer a wide range of scientific purposes that include studies of nucleosynthesis, the chemical evolution of the Galaxy, the propagation of cosmic-rays in the interstellar medium, etc. In addition, abundances of radioactive isotopes can be used to determine the time scale of cosmic-ray acceleration and transport. While *"primary"* cosmic-rays are considered as samples of matter from outside the solar system, to understand their history the study of the so called *"secondary"* cosmic-rays produced by break up of heavier nuclei in collision with interstellar material is also necessary. The iron group, Mn, Co and Ni are of particular interest (Leske 1993).

The isotope ^{54}Mn, together with ^{10}Be, ^{14}C, ^{26}Al and ^{36}Cl, has been proposed as a cosmic-ray clock (Cassé 1973). In the laboratory, ^{54}Mn decays with a 312 day half-life via an allowed electron capture transition to the 835 keV level in ^{54}Cr, although it is energetically possible for ^{54}Mn to decay via second forbidden unique transitions to the ground states of ^{54}Cr and ^{54}Fe by positron (β^+) and electron (β^-) emission, as shown in Figure 1. As a high energy cosmic-ray, ^{54}Mn would be stripped of all its atomic electrons, its decay by electron capture would be prevented, and long β^+ and β^- half-lifes would thus be expected. This could allow ^{54}Mn to serve as a cosmic-ray chronometer, if the partial half-lifes could be measured. Cassé (1973), who first proposed ^{54}Mn as cosmic-ray chronometer, estimated $t_{1/2} \sim 2 \times 10^6$ yr and $t_{1/2} \sim 10^9$ yr for the β^- and the β^+ decays, respectively. Later Wilson (1978) estimated that the β^- decay half-life must be larger than 6×10^4 yr, but smaller than 10^7 yr. Although the β^- decay intensity is expected to be about two orders of magnitude larger than the β^+ decay, measurement of the β^- decay has been considered difficult, partly because in absolute terms it is weak, and its endpoint energy of 697 keV falls below the

spectrum produced by scattered conversion electrons. The weaker, but easier to detect, β^+ branch has been searched for and experimental upper limits of $<4.4 \times 10^{-8}$ (Sur et al. 1989) and $<5.7 \times 10^{-9}$ (da Cruz et al. 1993) have been established for the β^+ branching ratio. Assuming the same *logft* values for the β^- and β^+ decays and using the β^+ partial half-life one can estimate the partial half-life of the β^- decay. Sur et al. (1989) concluded that the β^- partial half-life must be greater than 4×10^4 yr. Later da Cruz et al. (1993) set the current lower limit of $>2.95 \times 10^5$ yr.

Grove et al. (1991) examined the implications of the various estimates of the ^{54}Mn β^- decay life-time for the ^{54}Fe abundance in cosmic-ray source material as well as for cosmic-ray propagation studies. They concluded that present cosmic-ray data in conjunction with the propagation model cannot establish the degree of ^{54}Mn decay. From the measurement of the relative elemental and isotopic abundances of iron-group cosmic-rays, assuming τ_{esc} = 10 Myr (Wiedenbeck & Greiner 1980) for the mean escape time, Leske (1993) suggested that $\tau_{esc} > 50\ T_{\beta^-}$. More recently, Duvernois (1996) has remeasured the cosmic-ray Mn isotopic abundance distribution and has concluded that the ^{54}Mn β^- decay partial half-life should lie in the range of $(1\text{-}2) \times 10^6$ years.

In this paper we present the results of an attempt to observe the β^- decay directly using a magnetic electron spectrometer. This momentum selective instrument in combination with multiparameter data collection and sophisticated data analysis technique results in an upper limit, independent of *logft* assumptions.

2. β^- MEASUREMENTS

2.1. EXPERIMENTAL CONSIDERATIONS

The absence of suitable radiation in ^{54}Fe coincident with the ^{54}Mn β^- decay requires the *direct* measurement of the β^--energy spectrum. Since the β^--branch is expected to be very weak, any physical process producing a continuum even at low levels could interfere with the measurements. Furthermore, if the β-ray detector is even weakly sensitive to radiation such as γ-rays, the achievable sensitivity could be limited because the γ-ray flux is very high compared to the electron flux. The main features of these processes which could hamper the measurements are summarised in Table 1. They include:

(a) Electrons which deposit part of their energy in the detector. The discrete conversion electron lines from the 835 keV E2 transition in ^{54}Cr have an intensity about hundred times larger than the expected β^- decay. While the conversion peaks will be well resolved from the β^- spectrum, some of the conversion electrons will deposit only part of their energy in the Si(Li) detector, producing a continuum up to the primary energy. The probability for this process (backscattering) is dependent on factors such as angle of incidence, but in general is about 20% (Kalef-Ezra et al. 1982).

(b) Electrons which scatter within the source or on the internal surfaces of the spectrometer before reaching the detector.

(c) "Shake-off" electrons, caused by the sudden change in the electrostatic field of the nucleus when an electron is emitted because of internal conversion (Rao 1975) or electron capture (Freedman 1974) resulting in different spectrum shapes. The probability per K capture for double K-shell ionisation in the electron capture of ^{54}Mn has been measured at $3.6(3) \times 10^{-4}$ (Nagy and Schupp

1984), which is about hundred times larger than the expected β^- decay intensity, but is concentrated at low energy, so that the intensity at 90% of the maximum energy of 542 keV has dropped by a factor of $\sim 10^6$. The intensity of the shake-off electrons following internal conversion is about four orders of magnitude weaker than the electron conversion itself (Rao 1975).

(d) Electrons produced by Compton-scattering of the 835 keV γ-rays which can produce electrons up to an energy of 639 keV. While the total cross section depends on the Z-value of the scatterer, the shape of the energy spectrum will be determined by the scattering geometry.

(e) Continuum electrons from other beta emitters, which might be present as weak contaminants in terms of absolute activity, but whose β^- branches might be relatively strong.

(f) Direct interactions between the primary 835 keV γ-photons emitted in the ^{54}Mn EC-decay or scattered photons, producing signals up to the primary γ-ray energy. (While the detector is well shielded, the intensity of the 835 keV γ-rays is 10^5 times greater than the expected β^- branch.)

(g) Interactions of various parts of the spectrometer with γ-rays from laboratory background.

Auger electrons following the ^{54}Mn electron capture fall below of our detection cut-off of 25 keV. β^+-particles from the decay of ^{54}Mn are weak, and although they will have a maximum energy of 355 keV, they are discriminated against by the transport properties of the spectrometer, as discussed later.

2.2. SOURCE PREPARATION

Radioactive ^{54}Mn material dissolved in HCl was purchased from the New England Nuclear Company and kept in storage for approximately one year to allow short lived activity to decay. Further chemical purification was applied to reduce ^{65}Zn, ^{60}Co and ^{22}Na contamination using a procedure described by Sur et al. (1989). Several drops of the liquid was then deposited on a 600 $\mu g/cm^2$ mylar foil mounted on an aluminium frame (19 mm by 19 mm in area and 0.5 mm thick, with a 12.7 mm diameter central hole). The activity of this source was 4.8 μCi. Subsequent evaluation of the measurements revealed that Compton-scattering within the source material was significant, some of which was attributed to residues from the chemical purification. Compton-scattering from the source frame was also found to be a problem.

A stronger source (12.7 μCi) was prepared directly from a batch of ^{54}Mn material without any additional chemical purification. (The only detectable radioactive contamination was ^{60}Co at a level of 3.9×10^{-5} of the ^{54}Mn activity.) Compton scattering from the target frame were reduced by changing to a 0.2 mm thick rectangular mylar frame, 29 mm long and 19 mm wide, the largest area that could be accommodated with the existing target system. The central hole was expanded to a 22 mm by 15 mm rectangle, to minimise the material close to the ^{54}Mn activity. This source arrangement was used in the final measurements.

2.3. LENS SPECTROMETER DESCRIPTION AND MODIFICATION

Electrons were transported in the magnetic field of the superconducting solenoid described by Kibédi et al. (1990), operated in lens mode. That arrangement uses the baffle system, shown in Figure 2, consisting of two axial absorbers, a diaphragm and a spirally cut paddle wheel baffle so that β-particles which reach the detector are forced to traverse two orbits (loops). The maximum detection efficiency is ≈3% of 2 π solid angle.

The current to the solenoid is produced by a computer controlled power supply. For any chosen current the magnetic field will have a fixed value and thus the accepted electron momenta will cover a narrow range. To cover a broader range the field was swept between 80 gauss and 1530 gauss, allowing collection of electrons with energies between ~25 keV and ~1 MeV. Sweeping reduces the detection efficiency, depending on energy, to 0.1 - 0.5 % of 2π solid angle.

The direction of the field was chosen so that the paddle wheel baffle intercepted positrons and not electrons which spiral in opposite directions. The efficiency of the discrimination was tested directly by reversing the field to select positrons and then observing the reduction in the number of conversion electrons. (For the 662 keV conversion electrons in ^{137}Cs for example, a suppression factor of 2.6×10^3 was observed.)

Electrons were detected with a 200 mm^2 area and 3 mm thick, cooled, Si(Li) diode, located on axis, 35 cm from the source. The energy resolution measured for the 835 keV K conversion electron line was ~2.4 keV.

Singles γ-rays were recorded in a Compton-suppressed Ge detector, located perpendicular to the solenoid axis, ~25 cm from the source. In some cases coincidence γ-rays were recorded with a second Ge detector inserted into the solenoid tube, opposite the lens and ~3 cm from the source.

Initial measurements were performed using the solenoid in the form described by Kibédi et al. (1990). A relatively intense continuum was observed, equivalent to a β^- branch of $\sim 5\times10^{-4}$, but evaluation of the shape of the spectrum and other experimental tests traced the source of these electrons to Compton scattering from 835 keV γ-rays. From trajectory calculations, a number of surfaces were identified which could contribute to the background of multiple electron scattering and Compton scattering of γ-rays. To improve the system, the internal surfaces were coated with low Z-material (Teflon) and the geometric design of the axial absorbers and their supports were changed to minimise the amount of material exposed to γ-rays and electrons, and the possibility of scattering into the acceptance of the spectrometer.

The measurements were performed in the target area of the ANU 14UD accelerator during beam-off periods. The local room background produced a count rate of <0.5 counts/min in the Si(Li) detector, most of which could be filtered out using the analysis techniques described below.

While details of the modifications will be described in a separate paper (Kibédi et al. 1996), some important aspects of the data analysis techniques which resulted in an increased sensitivity will be presented.

2.4. DATA COLLECTION

The data were recorded in *event-by-event* mode and the digitised pulse information included *(a)* electron energy, *(b)* singles γ–ray energy, *(c)* coincidence γ-ray energy, *(d)* magnet power supply control signal, *(e)* magnetic field measured with a Hall probe, *(f)* coincidence electron-γ time difference. While the energy and timing signals were recorded with 4096 conversion range, the magnetic field related quantities were measured with 2048 conversion range. Since the coincidence γ–ray detector was close to the source, it was found to be an unnecessary source of Compton scattering and was removed for the final measurement. ^{152}Eu and ^{137}Cs sources were used to calibrate the electron and γ–ray spectrometers for energy and efficiency. Calibration of the magnetic field, and its relationship to the Hall probe readings and magnet current settings has been determined in previous measurements using a 3-axis gauss meter at several points on the solenoid axis.

2.5. MOMENTUM SELECTION

An important advantage of the lens spectrometer is that, at a given magnetic field, only a part of the full β-spectrum is transported onto the Si(Li) detector (Kibédi et al. 1990). This is governed by the momentum resolution, Δp/p, which is a geometrical property of this type of spectrometer (Siegbahn 1966). Formulae relating the magnetic field to the measured electron energy are given by Kibédi et al. (1990), and some aspects are repeated briefly here. The momentum selection we have used previously involves comparison of the magnetic field with the measured energy, and selection of those events which satisfy the expected functional relationship and are within the acceptable response of the spectrometer, determined by its momentum resolution. The relation between the transported β-ray energy (E)

and the magnetic field (B) can be defined over the [E,B] plane as (Kibédi et al. 1990):

$$B = C(r,\theta...) \times k\sqrt{E^2+2m_oc^2 E}\,/\,m_oc^2), \qquad (1)$$

where C is a coefficient which contains in effect the response function of the spectrometer as defined predominantly by the baffle geometry but also by factors such as source position and emmittance. The factor k is constant and m_oc^2 is the electron rest mass. As shown by Kibédi et al. (1990), *constant* upper and lower bounds can be specified for C, thus defining an area between two locii of field against energy, within which acceptable electron events, that is those which follow a principal trajectory through the spectrometer and also deposit their full energy in the detector, must fall. (See Figures 3 and 4 of Kibédi et al. (1990).)

Events caused by γ–rays in the Si(Li) detector are independent of field and therefore will be distributed uniformly along the magnetic field axis, while the events due to electrons which scatter from the detector will fall parallel with the energy axis in the [E,B] plane. In practical terms *momentum selection* is a procedure where the event-by-event data are tested against a two-dimensional [E,B] gate.

Considering a simple approximation to the transport of β-rays along helical orbits of path radius (curvature), *r*, and angle of emission θ with respect to the solenoid axis, C is approximately:

$$C = \frac{1}{r} \times \sin\theta\,. \qquad (2)$$

Because of the geometric acceptance of the spectrometer, r and θ are *correlated* and their extremes define a range of values from C=0.25 to 0.33. While the response function is essentially independent of energy, its centroid, and possibly width may differ for radiation produced at the centre or other part of the source, or from other parts of the spectrometer. This dependence which contains implicit in it, a further

correlation between the value of C and whether the trajectory is near the inner or outer envelope of principal trajectories, can be tested both experimentally and numerically. This was the basis of selection procedures more sophisticated than the coarse momentum selection mentioned above. This is illustrated schematically in panel (a) of Figure 3.

The response functions for three different energy gates are shown in Figure 3 on the right hand side. These spectra, plotted in logarithmic scale, illustrate the selectivity of the spectrometer for β-rays in terms of C. The spectrum gated by 344 K conversion electrons in the ^{152}Eu decay shows all the features of the momentum selection mentioned before. More than 93 % of the events fall in the acceptable region of C-values produced by conversion electrons and β-rays. The majority of the others having higher C-values. They can be associated with backscattering of higher energy (E>294 keV, the energy of 344 K conversion line) electrons. The contribution of the γ-background which will be independent of C, is rather weak. Similar projection of the ^{54}Mn data using the same gate on the beta-ray energy is shown in panel (c). It contains only a few counts in the acceptable region. The events distributed uniformly over the C-axis form the dominant feature, more evident in this case because the number of radioactive decays in the ^{54}Mn measurement was about 20 times of that in the ^{152}Eu case, the contribution of Compton scattered γ-rays thus being higher in the ^{54}Mn spectra. The bump at C ~ 0.5 - 0.6 is the contribution of the backscattering of the 835 keV conversion electrons. Finally the last panel shows the spectrum gated by conversion electrons of the 835 keV transition in ^{54}Cr. Since more than 98% of the counts falls into the acceptable region, this spectrum was used to determine the spectrometer response function.

3. EXPERIMENTAL RESULTS

3.1. EXPERIMENTS

Several tests were carried out, each of duration of 1-3 days, under different conditions, in order to determine possible sources of spectral distortion. These included:

(a) Lateral displacement of the source perpendicular to the solenoid axis to establish the relation between the geometrical origin and the centroid of C. Projections onto the C-axis with different source positions are compared in panel (a) of Figure 4.

(b) Reduction of the magnetic field in the first half of the baffle system as a means of decoupling the two longitudinal halves of the spectrometer. Projections onto the C-axis are compared with a measurement using the nominal field in panel (b) of Figure 4. The complete lack of field dependent events demonstrates the sensitivity on the geometrical origin. (Note that the distribution of the γ-ray events depends on the C-parameter due to the nonlinear boundaries of the C-E correlation illustrated in Figure 3.)

(c) Measurements with reversed magnet current to determine the suppression of positrons.

(d) Measurement of electron-γ coincidences as a probe of whether Compton-scattered γ-rays were correlated with detected electrons. The absence of a discrete peak in the summed energy of coincidence electrons and γ-rays indicated that such contributions were not significant. (Note that the γ-ray flux is much larger than the electron flux from the source.)

(e) Modifications to the size and composition of the target frame and source support to evaluate the contribution from scattering in the immediate vicinity of the source.

(f) Measurements with different sources and with ^{54}Mn sources of different strength and preparation.

(g) Measurements without a radioactive source to determine the contribution of room background.

The sources themselves were examined to check the distribution of the radioactive material by scanning the γ–ray activity using a narrow lead collimator and a Ge detector.

Although the physical modifications to the spectrometer itself resulted in the reduction of radiation scattering, the majority of residue events which were limiting the sensitivity were attributed to scattering of electrons produced initially by Compton-scattering of primary γ-rays on the target frame and within material of the radioactive source itself.

3.2. DATA EVALUATION AND ANALYSIS

The *event-by-event* data were sorted into [E,C] matrices. Using various gates on one axis, projections were made onto the other axis allowing the examination of different aspects of the correlation between energy and *C*. Representative spectra are shown in Figure 5, which compares projections on to the *C*-axis, under the conditions of the measurements after modification of the baffle system, but before changes to the source and its support (top frame), the final measurements (bottom frame), and some computer simulations (middle frame).

The magnitude of the improvements and the information implicit in the evaluation in terms of the response function C, is encapsulated in the comparison between the top and bottom frames. The data represent a projection of all events

over the 25 keV to 1 MeV region, while the shaded area is the projection with a gate on the conversion electrons of the 835 keV transition. In the top spectrum, most of the intensity is contributed by events other than those from the conversion, and those events are displaced predominantly to lower values of C than the conversion electrons. The fit to the total projection incorporates three Gaussians, the dashed one labelled B centred on the correct position, as defined by the projection of the conversion events, the other two (A and C) on either side.

The comparison of the data and components in the top and the bottom frame of Figure 5 shows the reduction of counts, which arise from unacceptable parts of the spectrum. Most importantly the distribution of events sensitive to the magnetic field is finally dominated by the conversion electrons. A further decomposition of these events in terms of residual contributions labelled as Gaussian A and C, will be pursued below.

3.2.1. COMPUTER SIMULATIONS

The middle frame of Figure 5 shows the results of Monte-Carlo computer simulations using models of the instrument and its transport properties. These are not expected to give an accurate representation, but should be indicative of the main features.

The calculated detection probability for the conversion lines from the source emitted under the same conditions is shown as the shaded area in the middle frame. (That the asymmetric shape does not reproduce experiment has been attributed previously to limitations in the model of Kibédi et al. 1990).

The curve, labelled as *frame*, in Figure 5 was produced by considering the target frame (of the same relative size as the original aluminium frame) as an

electron source with uniform intensity distribution. The results are in terms of absolute efficiency (based on a Monte-Carlo sample of more than 50000 particles). Only a small proportion of all events are transported, because of the tight response function with respect to position of the source, a property which was clear from the experimental tests involving lateral displacements of the source. The energy was fixed to 829 keV.

As can be seen, the position of the two side lobes produced in this simulation are comparable to the Gaussians A and C used in the upper panel.

3.2.2. SCATTERED INTENSITY

As noted above, the intensity residing in the side lobes in the original measurements was comparable to that of the conversion electrons. Since the detection efficiency of the spectrometer for events which originate from a displaced source is about six times smaller than for those which originate at the central source position, and if those electrons are produced initially by the scattering of γ-rays, the probability of Compton scattering on the frame must be about 0.1% for every 835 keV γ-ray emitted in the decay of ^{54}Mn. Due to the scattering geometry involved, most of the electrons would be ejected in the plane of the frame, which is perpendicular to the axis of the baffle system and the coincidence γ-ray detector. This would explain the very few electron-γ coincidences observed in the test measurements mentioned earlier.

These characteristics of the Compton scattering for the given geometrical conditions were supported by Monte-Carlo simulations of the process, and confirmed experimentally when the frame was replaced, resulting in a large reduction in the lobes.

3 .2 .3 . GAMMA-RAY BACKGROUND AND BACKSCATTERING TAIL

The flat background indicated in the top and bottom frames in Figure 5 is indicative of events uncorrelated with C, presumably γ-rays. These events have a source independent (laboratory background γ-rays) and a source dependent component (Compton scattered photons from the 835 keV γ-rays in the ^{54}Mn decay). In the case of the final measurements with the 12.7 μCi source, 72% of the γ-ray background is source dependent (as confirmed by a number of measurements without sources in place, and measurements without a magnetic field applied). The energy spectrum from such direct interactions of γ-photons in the Si(Li) detector decreases nearly exponentially with increasing energy.

Beta particles transported to the Si(Li) detector surface and then backscattered will deposit only a fraction of their initial energy. These particles will produce a nearly uniform distribution up to the incident energy (Kalef-Ezra et al. 1982). The corresponding events will appear in a banana shaped region in the [E,C] plane, which is parallel with the curve labelled B_{max} in Figure 3. The resulting contribution to the total C-projection is seen as a step at higher C-values, in the top and bottom spectra of Figure 5.

Because of the low statistics in the continuum region an algorithm was developed to determine the intensity distribution of the γ-ray background over the [E,C] plane using a mesh. (The region of acceptable events, indicated as shaded area in panel (a) of Figure 3, was excluded from the process). The description of global background was further improved by the incorporation of electron backscattering tail over the entire [E,C] matrix.

3.2.4. SPECTRUM UNFOLDING

Although not evident from visual inspection alone, detailed analysis showed that significant intensity still resided outside the expected distribution, probably from residual Compton scattering of γ-rays in the first half of the baffle system. In that context, it should be noted that the spectra in Figure 5 are dominated by the most intense single feature, the conversion lines, since no discrimination is made against energy in those cases. When the energy is restricted to be in specific region of the continuum, the relative contributions from different regions in C becomes more evident. By setting discrete digital gates in C, energy spectra can be produced from the matrices, and deconvoluted to generate spectra free of the partially resolved contaminants (see Kibédi et al. 1996 and Kerr 1994), in the manner common in γ-ray coincidence spectroscopy.

The resulting energy spectrum then was corrected for detection efficiency. Since the β-spectrum contains very few counts at low energies, the region up to 640 keV energy was plotted in 32 channel bins as shown in Figure 6.

The contribution of the different processes to this spectrum are listed in Table 1. The spectrum is dominated by the conversion electrons. A small residue of the backscattered events from the conversion electrons cannot be removed and is seen in Figure 6 as a tail at 750-829 keV energies. It is important to note that in the our multi-parameter data collection and analysis system the backscattered spectrum of the 835 keV conversion electrons and the expected ^{54}Mn β^- spectrum with an endpoint energy of 697 keV are completely resolved.

Four continuous components are identified in Figure 6. One is the β^- intensity, to be evaluated, the other three are shake-off, contaminant (^{60}Co) and

Compton events, only the last of which cannot be evaluated in absolute terms by scaling to measured quantities. The contribution of Compton ejected electrons from the source material itself and the backing foil was generated from Monte-Carlo simulations. The majority of such particles will point to directions parallel to the source surface and will not be recorded. By demanding *take-off* angles similar to those the source electrons, events could be produced in the ~420-640 keV region with the distribution indicated in Figure 6. Note that it has been arbitrary scaled to the edge at 640 keV, and is insignificant below 420 keV.

The spectrum of shake-off electrons in the electron capture decay of ^{54}Mn was calculated using a shape described by Primakoff and Porter (1953) and the double K-shell ionisation probability of Nagy and Schupp (1984). The energy spectrum of the ^{60}Co radioactive contamination is given for the intensity of 4×10^{-5} determined in γ-measurement. The ^{54}Mn β^-spectrum indicated is for an intensity of 2.7×10^{-5}.

In comparing the measured spectrum and the contribution of different radiations, there is an excess of intensity at energies below 200 keV. This may be caused by an unidentified pure β^- emitter which would not be seen in the γ-ray measurements. Alternative explanations, like spectral distortion at low energies are also possible. For example in this energy region multiple scattering within the source can be significant. For these reasons, since as can be seen in the Figure 6, only the 300-450 keV energy region is clean of contaminates, it has been used to set an upper limit on the ^{54}Mn β^- branching ratio.

3.2.5. EXPERIMENTAL UPPER LIMIT ON THE ^{54}Mn β^- BRANCHING RATIO

While the spectrum shown in the previous section provides a limit to branching, one further step can be taken to examine the events which made up that continuum, and select those which satisfy more precise conditions. The spectrometer response function, a Gaussian centred at C=0.2885 with a width of $\Delta C=0.0279$, determined from a projection of 835 keV conversion electrons, has been used to define the acceptable region. The position of the side lobes (assigned mainly to Compton electrons) has been determined by fitting two additional Gaussians of the same width. This is illustrated in Figure 7 (a). (It also shows the contribution of the 835 keV conversion electrons as a hatched area.) The same sort of fit (with fixed position and width for the Gaussians) was carried out to the projection of the 300-450 keV energy region as shown in Figure 7 (b). The area of the acceptable region defined by the Gaussian at C=0.2885 contains 223 (±53%) counts, compared to a total of 3.54×10^4 conversion electrons from 8.7×10^{10} primary decays. A higher peak area is obtained as shown in Figure 7 (c), if the positions of the side lobes are allowed to vary. The contribution of the β-rays in the acceptable region is then 677 (±8%) counts.

The former area corresponds to an upper limit of $<1.4 \times 10^{-5}$ for the intensity of the β^- decay, while the latter one could be considered as conservative upper limit of $<2.7 \times 10^{-5}$. Using the later value the partial half-life of the β^- decay must be greater than 3.2×10^4 years.

4. COMPARISON WITH COSMIC-RAY OBSERVATIONS

The application of ^{54}Mn as a chronometer for measuring the mean escape time of iron-group cosmic-rays requires the knowledge of the isotopic composition of the source, the effects of cosmic-ray transport and the partial half-life of ^{54}Mn β^- decay.

Manganese has three isotopes, of which ^{55}Mn is stable, and ^{53}Mn and ^{54}Mn decay under normal conditions by electron-capture. As a fully-ionized cosmic-ray, ^{53}Mn would be stable. From the isotope measurements of the cosmic-rays, Leske (1993) obtained the relative abundance ratios of the ^{53,54,55}Mn isotopes, which are 1 : <0.25 : $1.28^{+0.32}_{-0.25}$. Duvernois (1996) found ^{53,54,55}Mn in the ratios of 1 : 0.28(±0.07) : 0.71(±019). By comparing these values with the source composition, and the yields expected from the spallation of primary ^{56}Fe nuclei, usually assumed to be similar to the solar values, one can determine the amount of ^{54}Fe created in the decay of ^{54}Mn during propagation. Webber, Kish and Schrier (1990) found that the spallation yields of ^{53,54,55}Mn from proton interactions with 56Fe are nearly equal. Leske (1993) evaluated the effect of ^{54}Mn/^{53}Mn and ^{54}Fe/^{56}Fe ratios for a range of assumed source abundances and the ^{54}Mn half-life. It was shown, that based on the isotopic measurements alone one can set a lower limit of 50 for the τ_{esc} / $T_{1/2}$(^{54}Mn β^-) ratio. Using our lower limit for the ^{54}Mn β^- half-life of $T_{1/2} > 3.2 \times 10^4$ years one obtain a lower limit of $\tau_{esc} > 1.6$ Myr for the cosmic-ray confinement time.

In Table 2 we compare our determination of τ_{esc} with those found in other investigations involving different radioisotopes as cosmic-ray chronometers. In a recent article Wiedenbeck & Leske (1995) analysed the available results on the isotopic composition of iron-group galactic cosmic-rays. The comparison of the source composition of galactic matter derived from the cosmic-ray

experiments and predictions of the propagation model (Wiedenbeck & Leske 1995), does not rule out the existence of a relatively short half-life for the ^{54}Mn β^- decay.

References

Cassé, M. 1973, ApJ, 180, 623

da Cruz, M. T. F., et al. 1993, Phys. Rev., C48, 3110

Duvernois, M. 1996, Ph.D. thesis, Univ. of Chicago, and ApJ, submitted

Freedman, M. S. 1974, Annual Rev. Nuc. Sci., 24, 209

Grove, J. E., Hayes, B. T., Mewaldt, R. A., & Webber, W. R. 1991, ApJ, 377, 680

Kalef-Ezra, J., Horowitz, Y. S., & Mack, J. M. 1982, Nucl. Instr. and Meth., 195, 587

Kerr, M. 1994, Bsc thesis, Australian National University

Kibédi, T., Dracoulis, G. D., & Byrne, A. P. 1990, Nucl. Instr. Meth in Phys. Res., A294, 523

Kibédi, T., Kerr, M., Dracoulis, G. D., Norman, E. B., & Byrne, A. P. 1996, in preparation

Leske, R. A. 1993, ApJ, 405, 567

Nagy, H. J., & Schupp, G. 1984, Phys. Rev., C30, 2031

Primakoff, H., & Porter F. T. 1953, Phys. Rev., 89, 930

Rao, P. V. 1975, in *Atomic Inner-Shell Processes*, Vol. 2, (Academic Press New York), 1

Siegbahn, K. 1966, in Alpha-, Beta- and Gamma-Ray Spectroscopy, Vol. 1, (North-Holland), 148

Simpson, J. A., & Garcia-Munoz, M. 1988, Space Sci. Rev., 46, 205

Sur, B., Vogel K. R., Norman E. B., Lesko, K. T., Larimer, R.-M., & Browne, E. 1989, Phys. Rev., C39, 1511

Webber, W. R., Kish, J. C., & Schrier, D.A. 1990, Phys. Rev., C41, 547

Wiedenbeck, M. E., & Greiner, D. E. 1980, ApJ, 239, L139

Wiedenbeck, M. E. 1983, Proc. 18th Internat. Cosmic-Ray Conf. (Bangalore), 9, 147

Wiedenbeck, M. E. 1985, Proc. 19th Internat. Cosmic-Ray Conf. (La Jolla), 2, 84

Wiedenbeck, M. E., & Leske, R. A. 1995, Adv. Space Res., 15, 25

Wilson, L. W. 1978, Ph.D. theses, Univ. of California, Berkeley, LBL-7723

FIGURE CAPTIONS

FIG. 1. Schematic decay scheme for ^{54}Mn.

FIG. 2. Cross section of the lens spectrometer after modification.

FIG. 3. Mapping of *energy* vs *C-parameter* events.
(a) Distribution of correlated events (acceptable region of electrons) and uncorrelated events (γ-rays and backscattered electrons). The curves B_{max} and B_{min} indicate the upper and lower bounds of the magnetic field.
(b) Projection of C-values with a 288 - 298 keV gate encompassing the 344 K conversion electron line in the ^{152}Eu source measurement.
(c) Projection of C-values using the same gate in the ^{54}Mn measurement. (d) Projection of C-values gated by the 835 keV conversion electrons in the ^{54}Mn measurement. Note that no background has been subtracted.

FIG. 4. Correlation between transport properties and geometrical origin for β-rays.
(a) C-projection gated by 835 keV conversion electrons measured with source on axis and off-axis positions.
(b) The effect of the reduction of magnetic field in the first half of the baffle system. The spectrum of C-values, recorded with target coils off, shows no correlated events in the projection of 25 - 700 keV energy range, where the ^{54}Mn β^--rays are expected.

FIG. 5. Distribution of events along the C axis. The top panel shows the experimental spectrum recorded with the 4.8 μCi source with a 3-component fit superimposed. The shaded area is a projection gated by conversion electrons. The Gaussian marked as B corresponds to the *"acceptable" region* (B) and *side lobes* (A and C) can be attributed to electrons produced by instrumental distortions. The bottom panel shows the results of the experiment with the 12.7 μCi source. The middle panel is the calculated detection efficiency as a function of the C-parameter for electrons with different geometrical origin.

FIG. 6. The distortion free (unfolded) and efficiency corrected spectrum of ^{54}Mn the β^- measurements. The spectrum up to ~640 keV is plotted in 32 channel bins to reduce statistical fluctuations. The intensity of the contributions from the EC shake-off process and ^{60}Co radioactive contamination was known (see in the text). The intensity of the Compton-electron spectrum whose shape was obtained from computer simulation was normalised to the observed spectra in the 450-640 keV region. A ^{54}Mn β^--spectrum with an intensity of 2.7×10^{-5} has been superimposed.

FIG. 7. Assignment of the correlated events in terms of mapping on the [E,C] plane.

(a) Total projection of data fitted with the three Gaussians shown.

(b) Fit to projection of 300-450 keV region with Gaussian fixed in the position of those in (a).

(c) Fit with only the centre Gaussian is in position.

TABLE 1

Radiations in the ^{54}Mn β measurements and the methods used to suppress them. Counts are given for the experiment using the 12.7 μCi source.

Radiation		Energy [keV]	Intensity [per ^{54}Mn decay]	Suppression	Counts for 8.7×10^{10} decays[a] Total	300-450 keV
^{54}Mn β^-		≤697	1×10^{-5}		724	257
Conversion electrons	- 835 K	828.8	2.24×10^{-4}		32200	none
	- 835 L	834.1	2.08×10^{-5}		2900	none
	- Backscattered	up to 834.1	$<4 \times 10^{-5}$	- momentum selection[b]	<5300	none
Shake-off electrons	- EC decay	≤542	3.6×10^{-4}	- mainly low energy (<100 keV)	4400	<12
	- IC	≤828.8	$<2 \times 10^{-8}$		<8	<2
Compton-electrons		≤639.4	[c]	- low Z, low mass materials[d]	<2500	<120
Contaminants	- ^{60}Co	≤317.9	$<4 \times 10^{-5}$	- momentum selection[b] - chemical purification	<2000	<2
^{54}Mn γ-rays	- direct	834.8	0.99974	- axial baffles[e]	<20	none
	- scattered	≤834.8	2.2×10^{-6}	- large source detector distance[f]	210000	<43[g]
Room background γ-rays			$<8 \times 10^{-7}$	- momentum election[b]	80000	<21[g]

(a) Lens efficiency valid for β-particles emitted from the centre only. Count rates given in the 300 - 450 keV region are after sorting and unfolding the data.
(b) [E,C] events outside the region of *acceptable region* were rejected.
(c) An estimate of the intensity would involve the calculation of Compton-scattering and electron transport simultaneously.
(d) Spectrometer parts situated close to trajectories have been coated with Teflon.
(e) The two axial baffles with 11 cm thickness of lead suppress the 835 keV γ-rays by a factor of $\sim 2.5 \times 10^4$.
(f) The Si(Li) detector at 35 cm from the source substances a solid angle of $1.3 \times 10^{-4} / 4\pi$ only.
(g) Using the 2D background constructed over the [E,C] plane removes more than 95% of the γ-background from the region of the *acceptable events*.

TABLE 2

Cosmic-ray confinement time

Isotope	Half-life [Myr]	Confinement time [Myr]	Reference
^{10}Be	1.6	15^{+7}_{-4}	Simpson & Garcia-Munoz (1988)
		$8.4^{+4.0}_{-2.4}$	Wiedenbeck & Greiner (1980)
^{26}Al	0.87	$9.0^{+20.0}_{-6.5}$	Wiedenbeck (1983)
^{36}Cl	0.3	> 1	Wiedenbeck (1985)
^{54}Mn	> 0.04	> 2(*)	Leske (1993)
	> 0.295	> 15(*)	da Cruz et al. (1993)
	> 0.032	> 1.6(*)	This work

(*) Assuming $\tau_{esc} > 50\ T_{\beta^-}$.

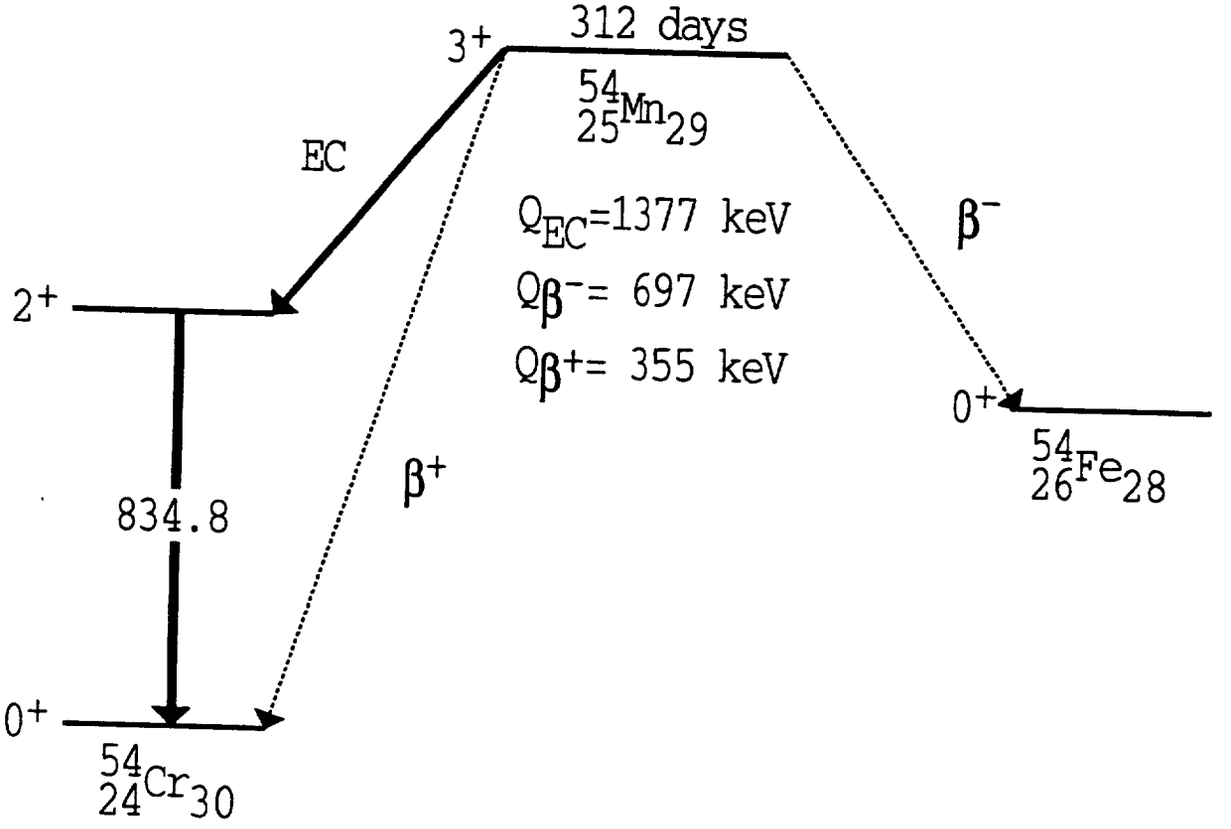
3+
312 days
$^{54}_{25}Mn_{29}$
EC
Q_{EC}=1377 keV
$Q\beta^-$= 697 keV
$Q\beta^+$= 355 keV
β^-
2+
0+
$^{54}_{26}Fe_{28}$
834.8
β^+
0+
$^{54}_{24}Cr_{30}$

Fig. 1

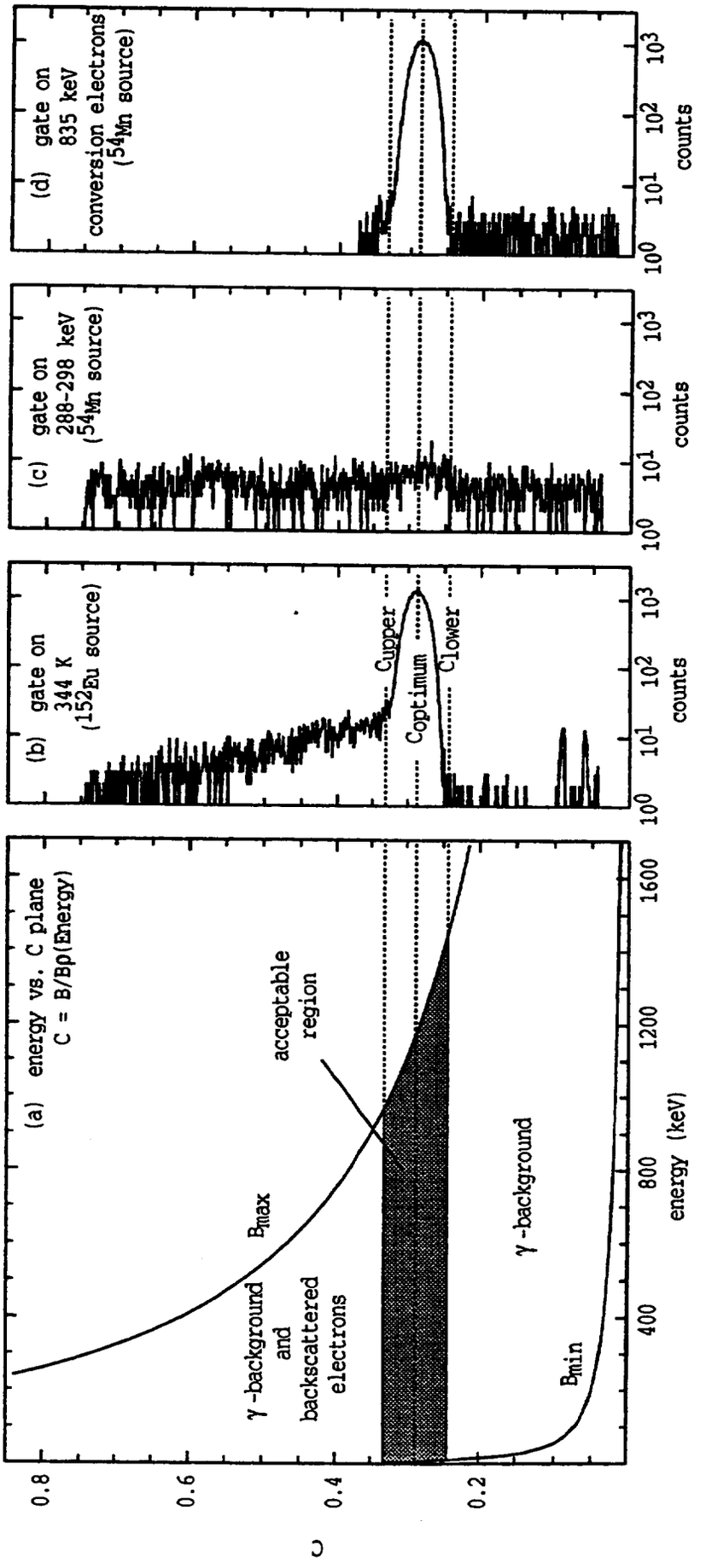
(a) energy vs. C plane
C = B/Bρ(Energy)
acceptable region
Bmax
γ-background and backscattered electrons
γ-background
Bmin
0.8
0.6
0.4
0.2
C
400
800
1200
1600
energy (keV)
(b) gate on 344 K (152Eu source)
Cupper
Coptimum
Clower
(c) gate on 288-298 keV (54Mn source)
(d) gate on 835 keV conversion electrons (54Mn source)
counts
100
101
102
103

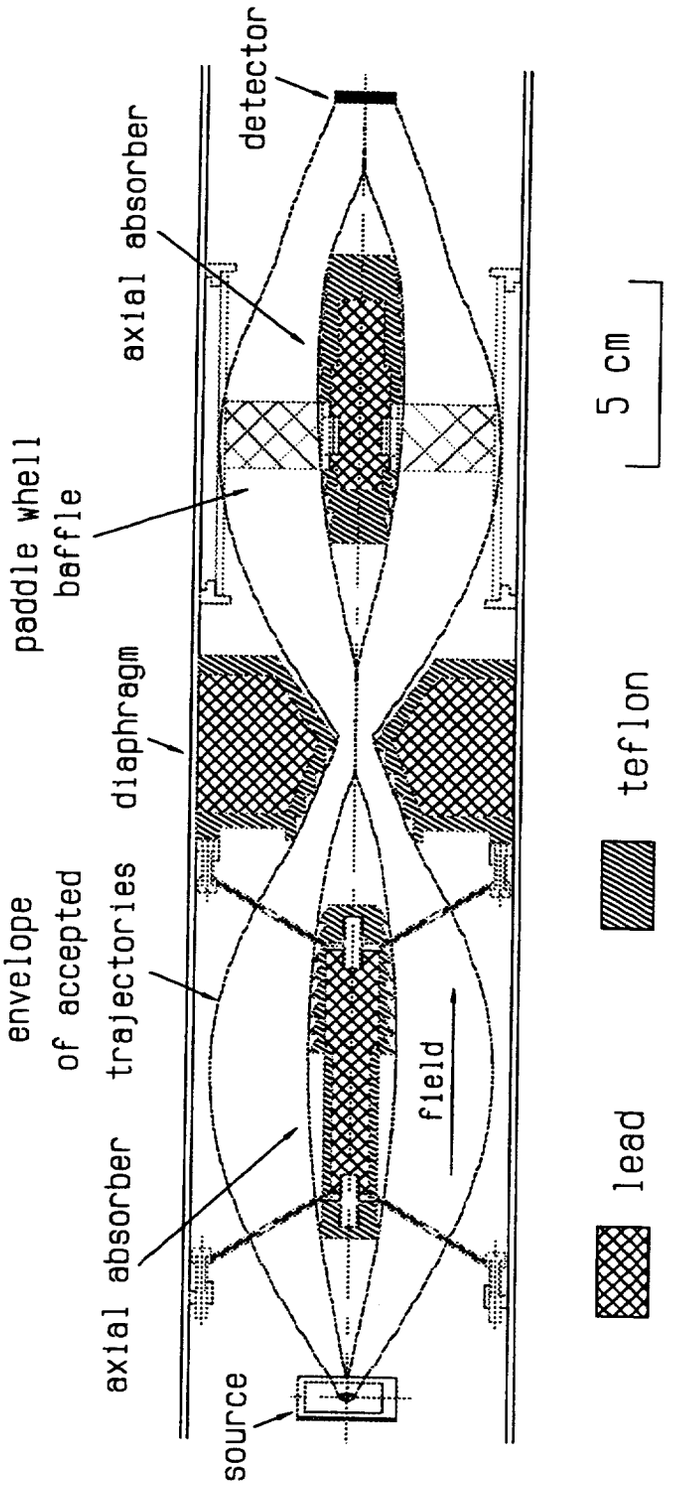
detector
axial absorber
paddle wheel
baffle
diaphragm
envelope
of accepted
trajectories
axial absorber
source
field
5 cm
teflon
lead

Fig. 2

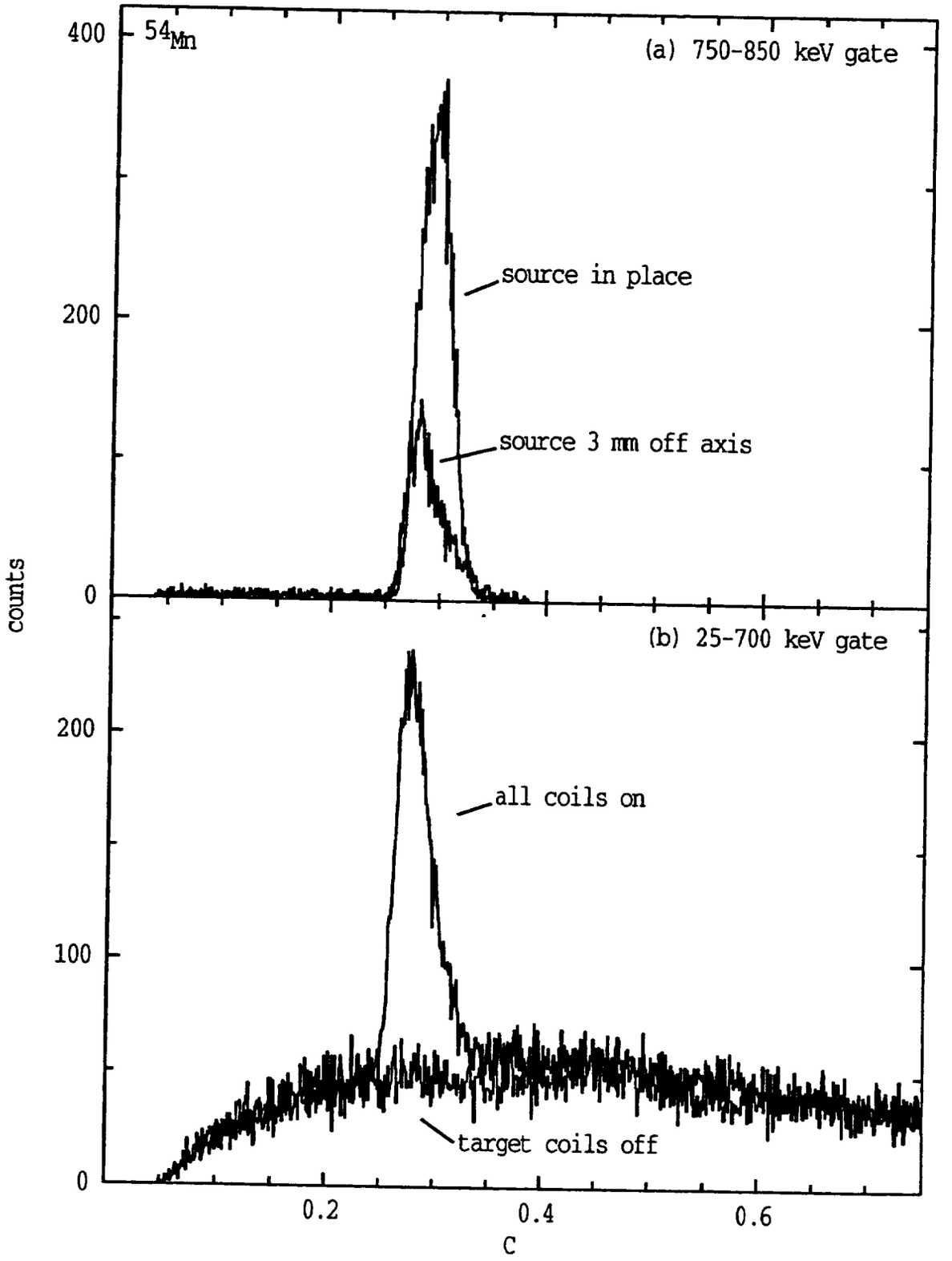
400
^{54}Mn
(a) 750-850 keV gate
source in place
200
source 3 mm off axis
0
counts
(b) 25-700 keV gate
200
all coils on
100
target coils off
0
0.2
0.4
0.6
C

Fig. 5

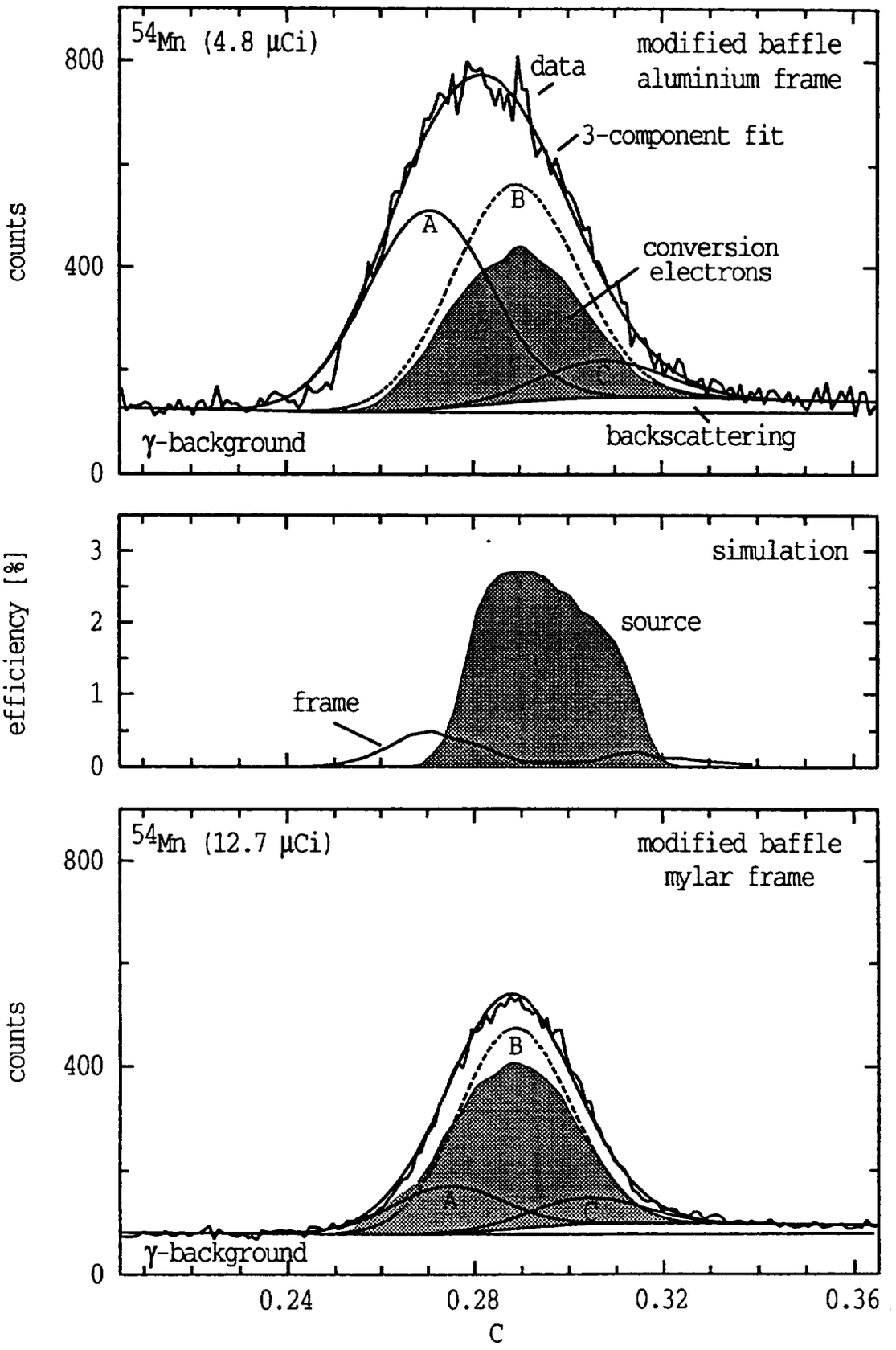
54Mn (4.8 μCi)
modified baffle
aluminium frame
data
3-component fit
A
B
conversion
electrons
γ-background
backscattering
counts
800
400
0
simulation
source
frame
efficiency [%]
3
2
1
0
54Mn (12.7 μCi)
modified baffle
mylar frame
counts
800
400
0
B
A
C
γ-background
0.24
0.28
0.32
0.36
C

Fig. 6

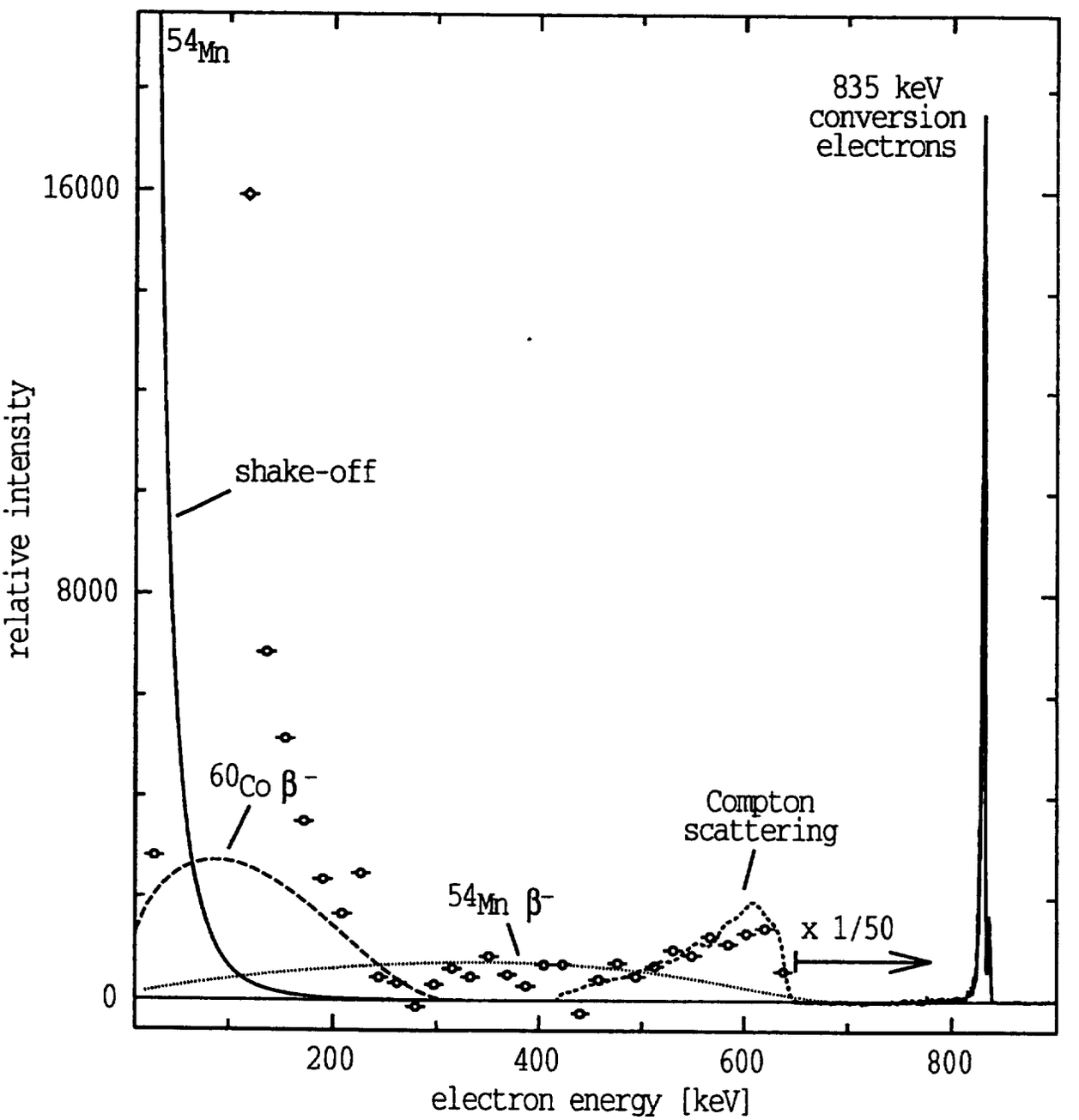
54Mn
835 keV
conversion
electrons
16000
8000
0
relative intensity
shake-off
60Co β-
Compton
scattering
54Mn β-
x 1/50
200
400
600
800
electron energy [keV]

Fig. 7

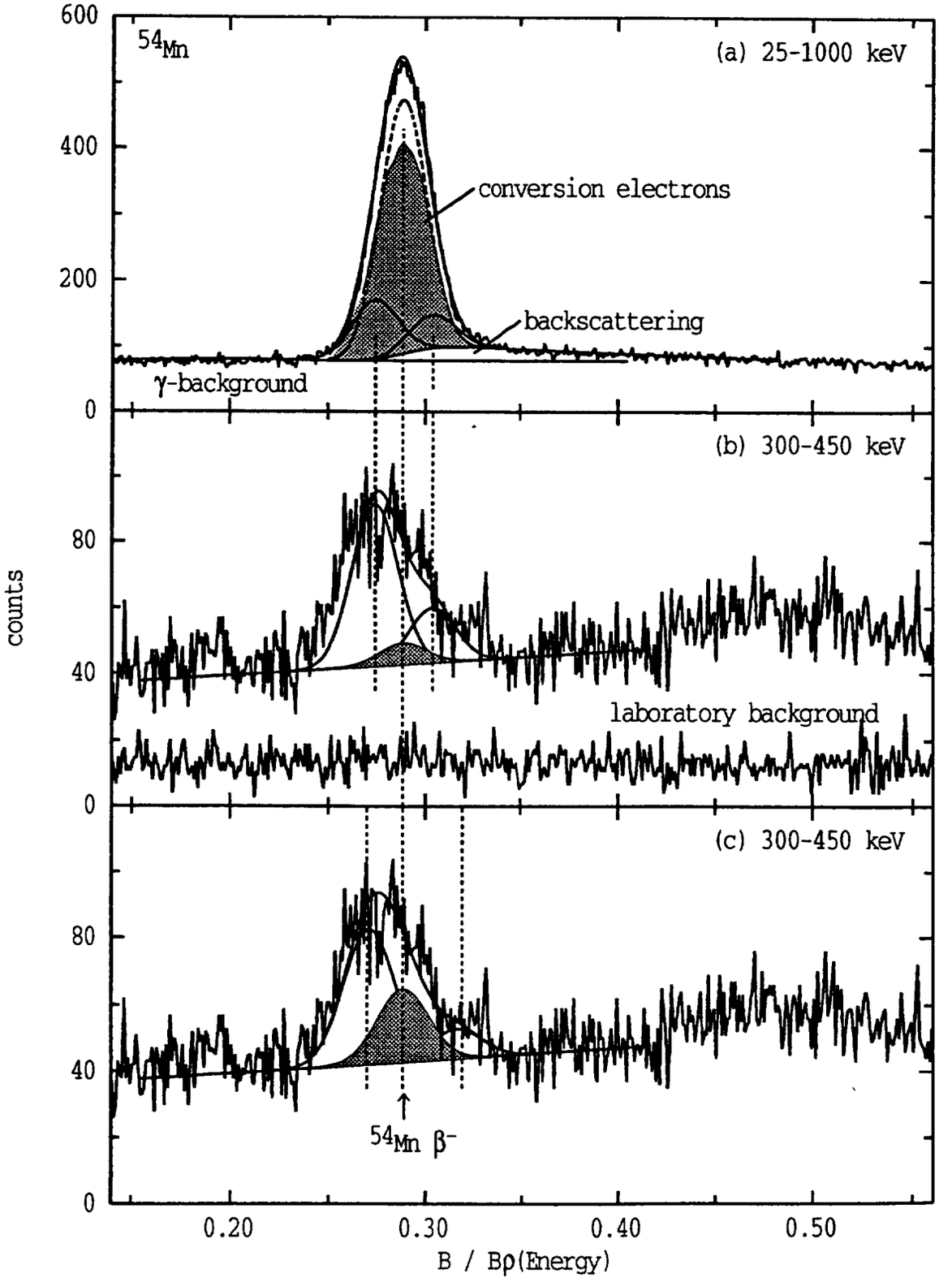
600
400
200
0
^{54}Mn
(a) 25-1000 keV
conversion electrons
backscattering
γ-background
(b) 300-450 keV
80
40
laboratory background
0
(c) 300-450 keV
80
40
^{54}Mn β$^-$
0
counts
0.20
0.30
0.40
0.50
B / Bρ(Energy)